Ann. Anim. Sci., Vol. 24, No. 4 (2024) 1197–1209 *DOI: 10.2478/aoas-2024-0038*

sciendo

EFFECT OF VITAMIN D_3 ON UTERINE MORPHOLOGY AND INSULIN SIGNALING IN A POLYCYSTIC OVARY SYNDROME (PCOS) RAT MODEL*

Kinga Kamińska[1,2], Marcelina Tchurzyk[1], Olga Fraczek[1], Agata Szlaga[3], Patryk Sambak[2,3], Szymon Tott[4], Kamilla Małek[4], Katarzyna Knapczyk-Stwora[1], Anna Błasiak[3], Agnieszka Rak[5], Małgorzata Grzesiak[1]♦

[1]Department of Endocrinology, Institute of Zoology and Biomedical Research, Faculty of Biology, Jagiellonian University, Gronostajowa 9, 30-387 Kraków, Poland
[2]Doctoral School of Exact and Natural Sciences, Jagiellonian University, prof. S. Łojasiewicza 11, 30-348 Kraków, Poland
[3]Department of Neurophysiology and Chronobiology, Institute of Zoology and Biomedical Research, Faculty of Biology, Jagiellonian University, Gronostajowa 9, 30-387 Kraków, Poland
[4]Department of Chemical Physics, Faculty of Chemistry, Jagiellonian University, Gronostajowa 2, 30-387 Kraków Poland
[5]Laboratory of Physiology and Toxicology of Reproduction, Institute of Zoology and Biomedical Research, Faculty of Biology, Jagiellonian University, Gronostajowa 9, 30-387 Kraków, Poland
♦Corresponding author: m.e.grzesiak@uj.edu.pl

Abstract

Polycystic ovary syndrome (PCOS) is a common endocrinopathy in women of reproductive age leading to infertility. Besides reproductive and hormonal disturbances, PCOS is often characterized by vitamin D_3 (VD) deficiency. This study aimed to determine the effect of VD on uterine histoarchitecture, the biochemical composition of gland secretions, and the insulin signal transduction pathway using a PCOS rat model. The experiment was conducted on four animal groups (n=8/group): control (C), VD supplemented (VD; 500 IU/day), letrozole-treated (PCOS; 1 mg/kg body weight), and VD-treated PCOS (PCOS+VD) group. Herein, VD supplementation did not improve histomorphometric parameters in the PCOS uterus, whereas clearly influenced sugar composition in uterine gland secretions, restoring their content to that observed in the C group. Furthermore, we found that VD can reduce peripheral and local uterine insulin resistance developed in the PCOS rats *via* activation of the phosphoinositide 3-kinase (PI3K)/protein kinase B (Akt) signaling pathway and subsequent glucose metabolism in the uterus. To sum up, the present results suggest a possible beneficial role of VD supplementation for the maintenance of uterus functions in PCOS rats.

Key words: vitamin D_3, insulin, PCOS, uterus, rat

Polycystic ovary syndrome (PCOS) is recognized as a common endocrinopathy affecting reproductive-age women and leading to infertility. Based on valid diagnostic criteria, it is characterized by oligoovulation and/or anovulation, biochemical and/or clinical hyperandrogenism, and ovarian cysts on ultrasound examination (Azziz et al., 2016). In addition, PCOS is associated with a wide spectrum of metabolic disturbances, including insulin resistance, hyperinsulinemia, type 2 diabetes, obesity, hyperlipidemia or non-alcoholic fatty liver disease (Li et al., 2019; Spremović Rađenović et al., 2022). Therefore, due to serious hormonal and metabolic alterations, the impact of PCOS on fertility impairment might go beyond well-studied ovarian aspects.

Recent findings showed abnormal uterine morphology and function in women with PCOS, resulting in pregnancy complications or even endometrial cancer (Piltonen, 2016). In PCOS patients, reduced endometrial receptivity to implantation marked by altered expression of genes encoding homeobox A10 protein (HOXA10) and αvβ3-integrin was observed (Hosseinzadeh et al., 2021). Both HOXA10 and αvβ3-integrin are down-regulated by testosterone, therefore their decreased endometrial expression in PCOS might be a result of hyperandrogenism (Jiang and Li, 2022). Furthermore, insulin resistance and hyperinsulinemia could inhibit decidualization contributing to disrupted endometrial receptivity in PCOS women (Hosseinzadeh et al., 2021). Regarding myometrium, morphological alterations as well as irregular contractions with higher frequency were reported during PCOS (Sajadi et al., 2018). Collectively, uterine abnormalities associated with PCOS seem to have a major impact on fertility and their molecular mechanisms require extensive investigation.

*This research was funded by the Priority Research Area BioS under the program Excellence Initiative – Research University at the Jagiellonian University in Kraków (grant no. U1U/P03/NO/14.87 to MG).

Previous research demonstrated that the uterus is a non-classical target tissue for insulin action, capable of developing local insulin resistance (Zhang et al., 2016). Insulin regulates glucose uptake after binding to membranous receptor (IR) and recruitment of insulin receptor substrate 1 (IRS1) followed by their phosphorylation. Subsequently, two predominant intracellular signaling pathways, *i.e.* the phosphoinositide 3-kinase (PI3K)/protein kinase B (Akt) and the mitogen-activated protein kinase (MAPK), are induced (Rahman et al., 2021). Activated Akt targets the glycogen synthase kinase 3 (GSK-3), inhibiting glycogen synthesis and thereby modulating its availability within the cell. Furthermore, the PI3K/Akt signaling pathway regulates the traffic of the insulin-sensitive glucose transporter 4 (GLUT4) to the cell membrane (Oróstica et al., 2016). A study by Li et al. (2017) conducted on uteri of rats with PCOS induced by letrozole described 148 differentially expressed miRNAs, which target genes involved in the insulin signaling pathways such as MAPK, PI3K/Akt and Ras, indicating that dysregulation of insulin-mediated intracellular signaling might contribute to uterine disturbances.

Increasing attention is being paid to vitamin D_3 (VD) supplementation as a promising therapy for insulin resistance in PCOS women. In general, the results of clinical and experimental trials suggest positive influence of VD on peripheral insulin resistance, but nothing is known about its local effect on the uterus (Kaminska and Grzesiak, 2021; Zhao et al., 2023). We hypothesize that VD supplementation decreases insulin resistance in the PCOS uterus, influencing PI3K/Akt pathway and thereby ameliorating uterine histoarchitecture. This study aimed to examine the effect of VD administration on: 1) plasma 25OHD, glucose and insulin concentration, and homeostatic model assessments, 2) uterine morphology, 3) biochemical composition of uterine gland secretions, 4) activation of insulin signaling pathway, and 5) GLUT4 protein abundance and localization in the uterus, using a letrozole-induced PCOS rat model.

Material and methods

Animals and experimental design

All procedures performed in this study were approved by the 2nd Local Institutional Animal Care and Use Committee (70/2021, Kraków, Poland) and conducted in accordance with the Directive 2010/63/EU of the European Parliament (2010) and the Act on the Protection of Animals Used for Scientific or Educational Purposes (2015).

Six-week-old female Wistar rats weighing 193.7±8.73 g were purchased from the Faculty of Pharmacy Jagiellonian University Medical College (Kraków, Poland). Animals were housed in controlled conditions of temperature, humidity and light (12 h light: 12 h dark cycle) with *ad libitum* availability of food and water. In this study, 32 rats were randomly assigned into the following groups: control (C; n=8), vitamin D_3-treated (VD; n=8), PCOS-induced by letrozole (PCOS; n=8), and PCOS-induced by letrozole with VD treatment (PCOS+VD; n=8). A daily treatment regime of 21 days included oral administration of compounds by gavage. The control group received vehicle treatment in the form of 2% (v/v) dimethyl sulfoxide (DMSO; Sigma-Aldrich, St. Louis, MO, USA) in rapeseed oil (1 mL/kg/day), the VD group received vitamin D_3 (500 IU/day; Vigantol (cholecalciferol) 20,000 IU/mL; P&G Health, GmbH, Germany), the PCOS group received letrozole (1 mg/kg/day; non-steroidal aromatase inhibitor; Sigma-Aldrich), and the PCOS+VD group received both letrozole and vitamin D_3. The doses were chosen based on our previous experiments (Kalamon et al., 2020; Grzesiak et al., 2021; Pich et al., 2023) as well as a literature review (Kafali et al., 2004; Lajtai et al., 2019). Rats were weighed daily, and estrous cyclicity was monitored by preparing vaginal epithelial cell smears. On the day of the experiment initiation, the animals remained in various spontaneous phases of the estrous cycle. Tissue and blood samples from acyclic animals in the PCOS and PCOS+VD groups were collected after 21 days of the experiment, whereas from animals in the C and VD groups on the first day of naturally occurring proestrus phase after 21 experimental days. PCOS induction was confirmed by the measurement of plasma testosterone concentration and the observation of ovarian cysts and lack of estrous cyclicity as we described recently in our paper using the same animal model (Pich et al., 2023).

Blood and uterine sample preparation

Blood and uterine samples were collected between 1:00 and 3:00 pm during proestrus in the C and VD groups and from acyclic rats in the PCOS and PCOS+VD groups. Animals were deeply anesthetized by inhalation of 4% isoflurane (Aerrane; Baxter, Warsaw, Poland) in the enclosed chamber. After verifying the depth of anesthesia through the absence of the corneal reflex, the animals were decapitated. Blood was withdrawn through the orbital sinus in a tube and centrifuged at 4000 *g* for 10 min at 4ºC. Plasma was separated and immediately stored at –20°C for further analyses. Uteri from each animal were harvested and weighed. The middle part of uterine horns was snap-frozen in liquid nitrogen for protein isolation or fixed in 10% buffered formalin for routine histology (Gomori trichrome and Periodic Acid–Schiff (PAS)/Alcian blue staining), Fourier transform infrared (FTIR) spectroscopy and immunofluorescence.

Uterine morphological parameters analysis

Paraplast-embedded 5-µm-thick sections after deparaffinization and rehydration, were immersed in Weigert's iron hematoxylin solution for 7 min and Gomori trichrome for 10 min. Stained sections were dehydrated, mounted using dibutylphthalate polystyrene xylene (DPX; Sigma-Aldrich) and coverslipped. Digital images from at least 10 slides of each experimental group were taken using a Nikon Eclipse E200 microscope with Digital Camera Nikon COOLPIX 5400 (Nikon, Tokyo,

Japan). The measurement of morphological parameters such as uterine lumen diameter, thickness of luminal (LE) and glandular (GE) epithelium as well as endometrium and myometrium was performed using ImageJ software (National Institutes of Health, Bethesda, MD, USA). 6–10 measurements were conducted per each section from different animals.

PAS/Alcian blue staining

Slides were stained with Alcian blue for 15 min, washed and then treated with 1% (w/v) periodic acid for 5 min. Then sections were stained with Schiff's reagent for 10 min, washed in running tap water, stained with hematoxylin, dehydrated, mounted in DPX and coverslipped. Uterine sections were analyzed under a Nikon Eclipse E200 microscope and representative images from each examined group were collected.

FTIR spectroscopic imaging and data analysis

IR images were recorded with a Varian 620-IR microscope coupled with a 670-IR spectrometer equipped with a 128 × 128-pixel focal plane array (FPA) detector (Agilent, Santa Clara, California, USA). IR images were acquired in transmission mode by illumination of samples through a Cassegrain 15× objective (NA: 0.62) and technological solution enhancing spatial resolution (spatial resolution of 3.0 µm at 2500 cm^{-1}). In this setup, IR image covers an area of 140 µm × 140 µm and is consistent of 16 384 spectra. All FTIR spectra were recorded by 128 co-scans in the region of 3600–900 cm^{-1} with a spectral resolution of 4 cm^{-1}. Measurements setup and data collection were performed using the Varian Resolutions Pro software.

Pre-processing of FTIR spectra and chemometric analysis were performed using CytoSpec (ver. 2.00.01), MatLab (R2015a, Natick, Massachusetts), and Origin (ver. 2018b, OriginLab, Northampton, Massachusetts) software. First, FTIR spectra were denoised with the use of principal component analysis (PCA; 17 PCs) and then vector normalized (1790–920 cm^{-1}). Next, second derivative IR spectra were calculated with a Savitzky-Golay algorithm (13 points) and corrected with Extended Multiplicative Signal Correction (EMSC) in the entire spectral region. Before further chemometric analysis of the IR image, we visually localized single glands and cut them off from the image (Figure 1 A). Unsupervised hierarchical cluster analysis (UHCA) was executed in the spectral region of 970–1770 cm^{-1} by using second derivative FT-IR spectra. Spectral distances were computed as D-values and individual clusters were extracted according to a Ward's algorithm. The number of classes was selected to separate the GE from its secretions (blue and red pixels in the HCA map, respectively, Figure 1 A). Normal and second derivative FTIR spectra were extracted from the calculated UHCA classes. The spectral interpretation was carried out for the spectra of the secretions only. These traces were averaged for each experimental group and displayed with the Origin software. The variation within the experimental groups is shown for second derivative spectra as standard deviation (± SD).

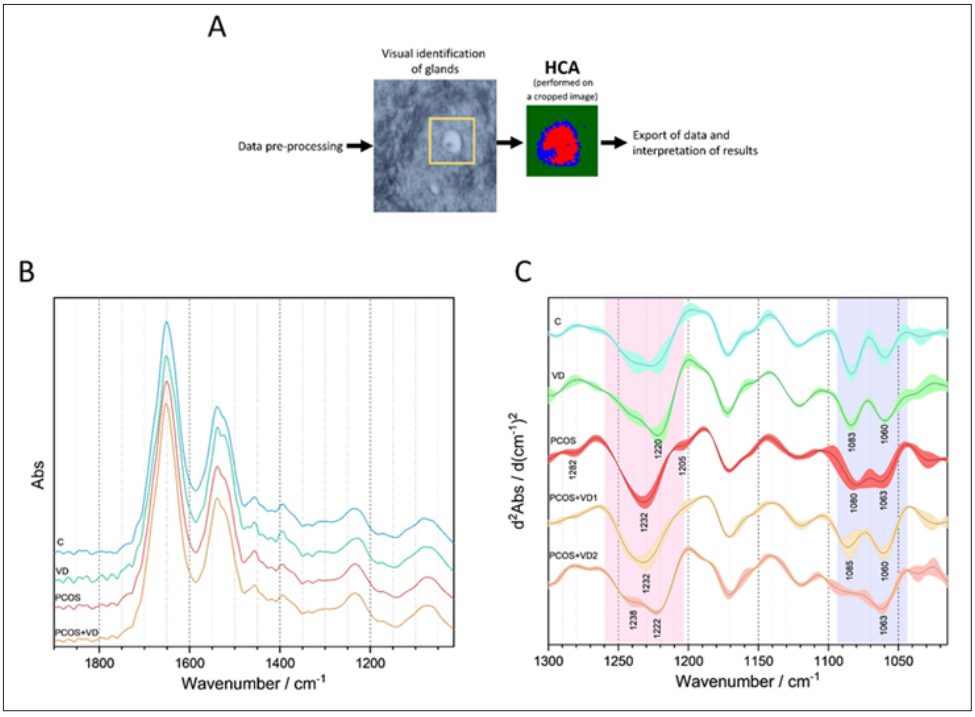

Figure 1 A schematic procedure used in the analysis of spectroscopic results (A). Averaged normal Fourier transform infrared (FTIR) spectra in the region of 1000–1900 cm^{-1} obtained for each studied group (NC: 11, NVD: 6, NPCOS: 14; NPCOS+VD: 11) (B). Averaged second derivative FTIR spectra of the uterine gland secretory fluid. Shading of the spectral traces represents standard deviation within the experimental groups (C). C, control group; VD, vitamin D_3-treated group; PCOS, polycystic ovary syndrome-induced group; PCOS+VD, PCOS-induced with vitamin D_3 supplementation group

Table 1. Primary and secondary antibodies used for Western blot

Antibody	Host species	Vendor	Catalog no.	RRID	Dilution
IR	Rabbit	Cell Signaling, Technology, Danvers, MA, USA	3025	AB_2280448	1:1000
p-IR	Rabbit	Cell Signaling, Technology, Danvers, MA, USA	3023	AB_2249189	1:1000
IRS1	Rabbit	Cell Signaling, Technology, Danvers, MA, USA	2390	AB_10692516	1:250
p-IRS1	Rabbit	Cell Signaling, Technology, Danvers, MA, USA	2385	AB_330363	1:250
PI3K	Rabbit	Cell Signaling, Technology, Danvers, MA, USA	4257	AB_659889	1:1000
p-PI3K	Rabbit	Cell Signaling, Technology, Danvers, MA, USA	17366	AB_2895293	1:1000
Akt	Rabbit	Cell Signaling, Technology, Danvers, MA, USA	9272	AB_329827	1:1000
p-Akt	Rabbit	Cell Signaling, Technology, Danvers, MA, USA	9271	AB_329825	1:1000
GSK-3α	Rabbit	Cell Signaling, Technology, Danvers, MA, USA	4337	AB_10859910	1:1000
p-GSK-3α	Rabbit	Cell Signaling, Technology, Danvers, MA, USA	9316	AB_659836	1:500
GSK-3β	Rabbit	Cell Signaling, Technology, Danvers, MA, USA	12456	AB_2636978	1:1000
p-GSK-3β	Rabbit	Cell Signaling, Technology, Danvers, MA, USA	5558	AB_10013750	1:500
GLUT4	Mouse	ProteinTech Group, Chicago, IL, USA	66846-1	AB_2882186	1:1000
β-actin	Mouse	Sigma-Aldrich, St. Louis, MO, USA	A2228	AB_476697	1:4000
Secondary anti-rabbit IgG	Goat	Jackson ImmunoResearch, Cambridge, UK	111-035-144	AB_2307391	1:10000
Secondary anti-mouse IgG	Goat	Jackson ImmunoResearch, Cambridge, UK	115-035-003	AB_10015289	1:10000

Abbreviations: IR, insulin receptor; p-IR, phospho-IR; IRS1, insulin receptor substrate 1; p-IRS1, phospho-IRS1; PI3K, phosphoinositide 3-kinase; p--PI3K, phospho-PI3K; Akt, protein kinase B, p-Akt, phospho-Akt; GSK-3**α**, glycogen synthase kinase-3α; p-GSK-3**α**, phospho-GSK-3**α**; GSK-3**β**, glycogen synthase kinase-3β; p-GSK-3**β**, phospho-GSK-3**β**; GLUT4, glucose transporter type 4; RRID, Research Resource Identifiers.

25OHD concentration

Plasma 25OHD concentration was measured by enzyme-linked immunosorbent assay (ELISA) using Total 25-OH Vitamin D ELISA Kit (cat. no 80987, Crystal Chem, Downers Grove, IL, USA) in a Labtech LT-4500 plate reader (Labtech International Ltd., Uckfield, UK) at 450 nm following the manufacturer's instruction. Assay sensitivity was 5.5 ng/mL over the range 10–160 ng/mL, and intra-assay and inter-assay coefficients of variation were less than 10.0%. All samples were analyzed in duplicate.

Glucose and insulin concentration, and homeostatic model assessments (HOMAs)

Glucose and insulin concentrations were assessed in blood plasma following animal fasting for 12 h before euthanasia. Fasting glucose (FG) concentration was determined by colorimetric method using the Glucose Oxidase Reagent (cat. no G7521, Pointe Scientific, Brussels, Belgium) according to the manufacturer's instruction using a spectrophotometer UV-1600PC (VWR, Radon, PA, USA). The detection limit was 1 mg/dL, and intra-assay and inter-assay coefficients of variation were 1.1% and 2.5%. Fasting insulin (FINS) concentration was determined using the Rat Insulin ELISA kit (cat. no 90010, Crystal Chem) according to the manufacturer's protocol. Assay sensitivity was 0.156 ng/mL over the range 0.156–10.0 ng/mL. The intra-assay and inter-assay precisions were less than 10.0%. A homeostatic model assessment of insulin resistance (HOMA-IR) and β-cell function (HOMA-β) were calculated using the formulas HOMA-IR = FG (mmol/L) × FINS (μU/mL)/22.5 and HOMA-β = (20 × FINS [μU/mL])/(FG – 3.5) (Moustafa et al., 2021).

Western blot

Total protein extraction and Western blot analysis were conducted as previously described (Grzesiak et al., 2021). Samples (20 μg) were separated by 10% (v/v) SDS-PAGE (Mini-Protean TGX Precast Gels; Bio-Rad Laboratories Inc., GmbH, München, Germany) and electroblotted onto a PVDF membrane (Trans-Blot Turbo Mini 0.2 μm PVDF Transfer Packs; Bio-Rad Laboratories Inc.) using a semi-dry Trans-Blot Turbo Transfer System (Bio-Rad Laboratories Inc.). The blotted membranes were blocked for 1 h at room temperature (RT) in 5% (w/v) non-fat dry milk containing 0.1% Tween20 followed by overnight incubation at 4°C with primary antibodies and then with respective secondary horseradish peroxidase-conjugated antibodies (Table 1) for 1.5 h at RT. Proteins were detected by chemiluminescence and images were captured with a ChemiDocTM XRS+ System (Bio-Rad Laboratories Inc.). Each membrane was stripped and reprobed with anti–β-actin or anti-vinculin (only for GLUT4) antibodies followed by respective secondary antibodies (Table 1). The bands were densitometrically quantified and normalized to their corresponding β-actin or vinculin bands using ImageJ software.

Immunofluorescence

Immunofluorescence staining was performed as described previously (Grzesiak et al., 2022). Briefly, an unmasking procedure with microwave heating in 0.01 M citrate buffer (pH 6.0) and blocking of non-specific binding sites with 5% (v/v) normal goat serum prior to immersion with anti-GLUT4 primary antibody (Table 1) was performed. After overnight incubation at 4°C in a humidified chamber, the antigens were visualized using

anti-mouse Alexa Fluor™ 488-conjugated secondary antibody for 1.5 h in the dark (cat. no. A-11001; Invitrogen, Carlsbad, CA, USA). Finally, sections were mounted in Vectashield Antifade Mounting Medium with 4′,6-diamidino-2-phenylindole (DAPI) (Vector Lab., Burlingame, CA, USA) and examined with an epifluorescence microscope Nikon Eclipse Ni-U with corresponding software. Negative controls were prepared by section incubation with non-immune mouse IgG (NI03, Calbiochem, Darmstadt, Germany) instead of primary antibody.

Statistical analysis

Statistical analysis was conducted using Statistica 13.3 software (StatSoft® Poland). Results are presented as the overall mean ± standard deviation (SD) for data of uteri weight, LE and myometrium thickness, hormonal and metabolic parameters as well as Western blot analysis or the overall mean ± standard error of the mean (SEM) for data of GE and endometrium thickness, and the uterine lumen diameter. The normal distribution of data was verified by the Shapiro-Wilk and Lilliefors tests. One-way ANOVA followed by the Tukey *post hoc* test was used to analyze uterine weight, LE and myometrium thickness, hormonal and metabolic parameters, and Western blot results. Nonparametric Kruskal-Wallis test was used to analyze GE and endometrium thickness, and the uterine lumen diameter. Differences were considered statistically significant when $P<0.05$.

Results

Effect of VD on hormonal and metabolic parameters

In the present study, we have assessed the effect of VD supplementation on the plasma 25OHD level. As expected, 25OHD concentration was the lowest in the PCOS group, when compared with the C, VD and PCOS+VD groups ($P<0.05$, $P<0.001$ and $P<0.001$, respectively). The greatest 25OHD level was found in the VD group that was significantly higher than in the C ($P<0.05$) group. In the PCOS+VD group, 25OHD concentration was markedly increased in comparison to the PCOS ($P<0.001$) and C ($P<0.05$) groups (Table 2).

Glucose concentration was higher in rats with PCOS in comparison to the C and VD groups ($P<0.05$ and $P<0.001$, respectively), while VD supplementation led to a significant decrease (PCOS+VD group; $P<0.05$). In the VD group, glucose level was markedly lower than in the C, PCOS and PCOS+VD groups ($P<0.05$, $P<0.001$ and $P<0.05$, respectively). Insulin level was greater in the PCOS group than in the C ones ($P<0.05$). Based on those results, calculated HOMA-IR was significantly greater in PCOS-induced animals when compared to the C, VD and PCOS+VD groups ($P<0.01$, $P<0.01$ and $P<0.01$, respectively), while HOMA-β was higher in the VD group than in the C groups ($P<0.01$) (Table 2).

Table 2. Hormonal and metabolic parameters of rats from control (C), vitamin D_3-treated (VD), polycystic ovary syndrome-induced (PCOS) and PCOS-induced with vitamin D_3 supplementation (PCOS+VD) groups

	C	VD	PCOS	PCOS+VD
25OHD (ng/mL)	11.53±1.62 a	32.78±4.3 b	3.86±1.03 c	27.9±4.72 b
Insulin (pmol/L)	2.17±0.51 a	3.34±0.93 ab	4.17±1.65 b	3.41±0.57 ab
Glucose (mmol/L)	9.69±0.59 a	8.36±0.53 b	12.34±0.75 c	10.3±1.14 a
HOMA-IR	0.12±0.024 a	0.177±0.048 a	0.326±0.128 b	0.201±0.039 a
HOMA-β (%)	1.006±0.207 a	1.584±0.477 b	1.181±0.51 ab	1.251±0.344 ab

All data are expressed as mean ± SD (standard deviation). The comparisons were performed in rows and means with different letters differ significantly. Means sharing the same letter are not statistically different. Means labeled with multiple letters "ab" are not statistically different than means labeled with "a" or "b". Data were analyzed by one-way ANOVA followed by Tukey *post hoc* test (n=8 rats per group). P value was considered significant when $P<0.05$.

Abbreviations: HOMA-IR, homeostasis model assessment of insulin resistance; HOMA-β, homeostasis model assessment of β cell function; 25OHD, total 25-hydroxyvitamin D

Table 3. Uterine histomorphometric parameters in rats from control (C), vitamin D_3-treated (VD), polycystic ovary syndrome-induced (PCOS) and PCOS-induced with vitamin D_3 supplementation (PCOS+VD) groups

	C	VD	PCOS	PCOS + VD
Uteri weight (g)	0.396±0.08 a	0.36625±0.02 a	0.145±0.01 b	0.186±0.015 b
Lumen (μm)	814.10±53.21 a	933.48 ±59.26 a	502.67±49.33 b	519.11±87.00 b
Thickness of LE (μm)	20.04±6.59 a	22.26±7.08 a	12.45±2.56 b	14.18±5.32 b
Thickness od GE (μm)	16.14±0.53 a	17.37±0.54 a	11.14±0.51 b	13.47±0.74 b
Thickness of E (μm)	485.78±22.33 a	437.64±27.79 ac	278.94±17.88 b	346.96±15.80 bc
Thickness of M (μm)	304.19±106.25 a	261.57±76.89 a	197.14±49.45 b	191.85±52.47 b

All data are expressed as mean ± SD (standard deviation) or SEM (standard error of mean). The comparisons were performed in rows and means with different letters differ significantly. Means sharing the same letter are not statistically different. Mean labeled with multiple letters "ac" is not statistically different than mean labeled with "a" or "c", while mean labeled with "bc" is not different from mean labeled with "b" or "c". Data for uteri weight, thickness of luminal epithelium and myometrium were analyzed by one-way ANOVA followed by Tukey *post hoc* test, while data for uterus lumen diameter, thickness of glandular epithelium and endometrium were assessed by Kruskal-Wallis test (n=8 rats per group). P value was considered significant when $P<0.05$.

Abbreviations: E, endometrium; GE, glandular epithelium; LE, luminal epithelium; M, myometrium.

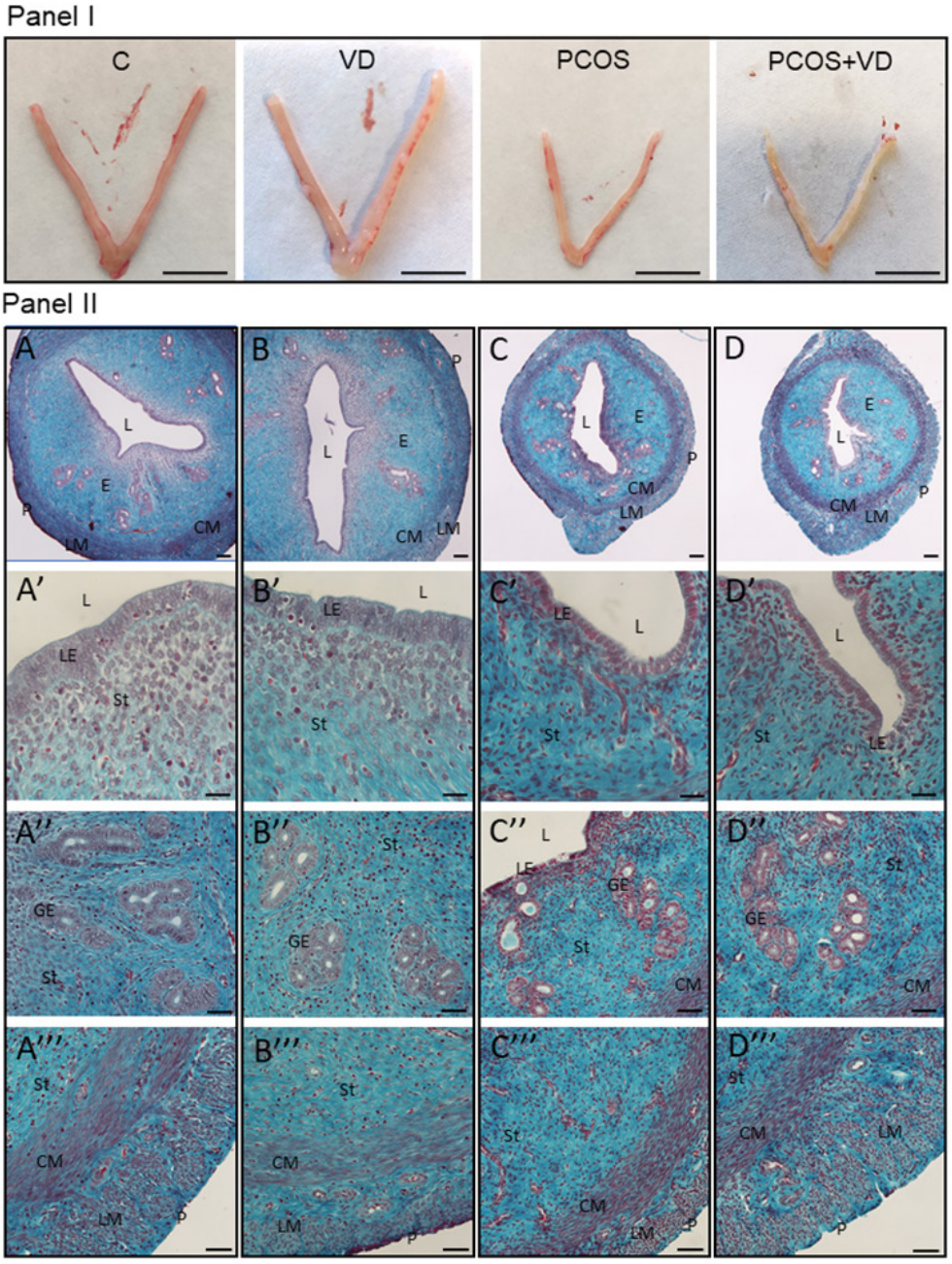

Figure 2. Panel I: Representative micrographs of uteri from the control (C), vitamin D_3-treated (VD), polycystic ovary syndrome-induced (PCOS) and PCOS-induced with vitamin D_3 supplementation (PCOS+VD) groups. Scale bar = 1 cm. Panel II: Representative micrographs of Gomori trichrome staining of uteri from the C (A-A‴), VD (B-B‴), PCOS (C-C‴) and PCOS+VD (D-D‴) groups. E, endometrium; GE, glandular epithelium; L, lumen; LE, luminal epithelium; CM, circular myometrium; LM, longitudinal myometrium; P, perimetrium; St, stroma. Scale bar = 100 µm (A-D), 25 µm (A'-D'), 50 µm (A''-D'', A'''-D''')

Effect of VD on uterine histomorphometric parameters

The analysis of uterine weight demonstrated a significant reduction in both PCOS and PCOS+VD groups when compared with the C and VD ones ($P<0.001$ and $P<0.001$, respectively) (Figure 2 Panel I; Table 3). Additionally, the uterine lumen diameter in the PCOS and PCOS+VD groups was smaller than that in the C ($P=0.0065$ and $P=0.0006$, respectively) and VD ($P=0.0002$ and $P=0.0005$, respectively) groups (Figure 2 A–D Panel II; Table 3).

Histological analysis confirmed the presence of typical uteri compartments (endometrium, longitudinal and circular myometrium, and perimetrium) in all examined groups (Figure 2 A–D Panel II). The thickness of the endometrium layer was markedly decreased in the PCOS group when compared with the C and VD groups ($P=0.00001$ and $P=0.00005$, respectively; Table 3). There was no differences between the PCOS and PCOS+VD groups, but the endometrium thickness in the latter was decreased when compared to the C group ($P=0.0004$; Table 3). Within the endometrium, the luminal (Figure 2 A'–D') and

glandular (Figure 2 A''–D'') epithelial cells were cuboidal in all analyzed groups with differences in their thickness. The thickness of both epithelia was similar between the PCOS and PCOS+VD groups and markedly lower than in the C ($P<0.001$ and $P<0.001$, respectively) and VD groups ($P<0.001$ and $P<0.001$, respectively) (Table 3). We also found that the thickness of the entire myometrium area was significantly decreased in the PCOS and PCOS+VD groups in comparison to the C ($P<0.001$ and $P<0.001$, respectively) and VD ($P<0.05$ and $P<0.05$, respectively) groups (Figur 2 A'''–D'''; Table 3).

Effect of VD on biochemical composition of uterine gland secretory fluid

PAS reaction for neutral polysaccharides (stain in magenta/purple) and Alcian blue staining for acidic polysaccharides (stain in blue), showed differences in the composition of the uterine secretions between examined animals. In the C (Figure 3 A) and VD (Figure 3 B) groups, uterine gland secretory fluid and secretions on the LE revealed positive Alcian blue staining. In the PCOS (Figure 3 C) and PCOS+VD (Figure 3 D) groups, the positive staining was found only within uterine glands. However, apart from the presence of blue staining, the positive PAS reaction was also observed in those groups. In details, magenta-colored staining was noted in the PCOS group (Figure 3 C), whereas in the PCOS+VD group the staining was purple (Figure 3 D).

To perform a more detailed analysis of the biochemical composition of uterine gland secretory fluid, FTIR technique was employed. The obtained spectra showed a profile typical for samples of biological origin (Figure 1 B). They were dominated by amide I and II bands at 1650 and 1538 cm^{-1}, indicating the presence of proteins. Another protein region appeared from 1340 to 1200 cm^{-1} (amide III) and indicated collagens. Since the tissue cross-sections were deparaffinized before IR imaging, we did not expect lipids to contribute to the spectral profiles. Vibrations of CO and COH bonds in carbohydrates of various classes exhibited bands in the region below 1300 cm^{-1} and the comparison of their relative intensities concerning the protein bands suggested that they are predominant components of the gland (Figure 1 B). The variability in the composition of sugars between the experimental groups was observed in the second derivative FTIR spectra, in particular in two regions of 1260–1200 cm^{-1} (region 1) and 1100–1050 cm^{-1} (region 2) as shown in Figure 1 C. The overlapped spectra cannot be unequivocally assigned to specific sugars but can be attributed to their classes. Bands in region I (1240, 1232 and 1222 cm^{-1}) originate from the vibrations of the COH and OSO^{3-} group in glycosaminoglycans (GAGs), proteoglycans (PGs), and glycoproteins (GPs). Their presence also contributes to the amide bands of proteins. In region 2, the bands at 1080 and 1060 cm^{-1} are assigned to polysaccharides (including phosphorylated moieties) and total content of sugars, respectively. The 1030 band cm^{-1} is an IR signal of monosaccharides, but it does not significantly differ between the groups (Figure 1 C) (Servaty et al., 2001; Bavington et al., 2004; Lewis et al., 2013; Staniszewska et al., 2014; Wiercigroch et al., 2017; Mohamed et al., 2020).

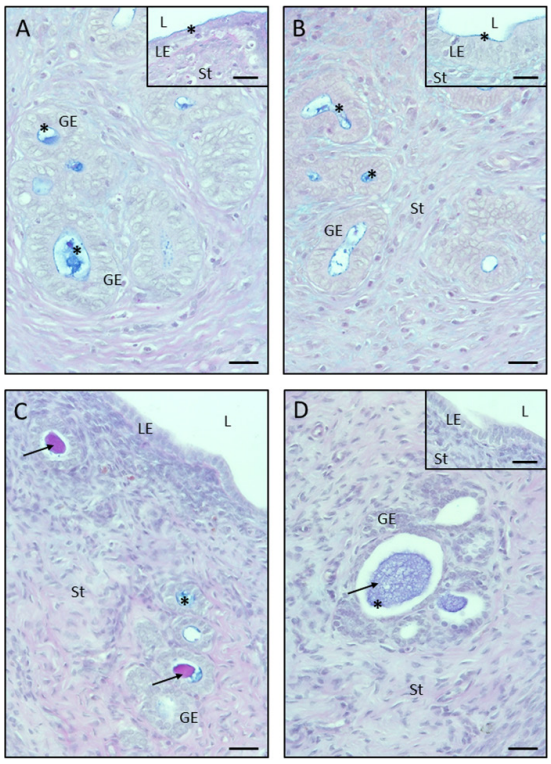

Figure 3. Representative micrographs of PAS and Alcian blue staining of uteri from control (A), vitamin D_3-treated (B), polycystic ovary syndrome-induced (C) and PCOS-induced with vitamin D_3 supplementation (D) groups. Arrows indicate positive PAS staining (magenta/purple color), while asterisks indicate positive Alcian blue staining (blue color). GE, glandular epithelium; L, lumen; LE, luminal epithelium; St, stroma. Scale bar = 25 µm

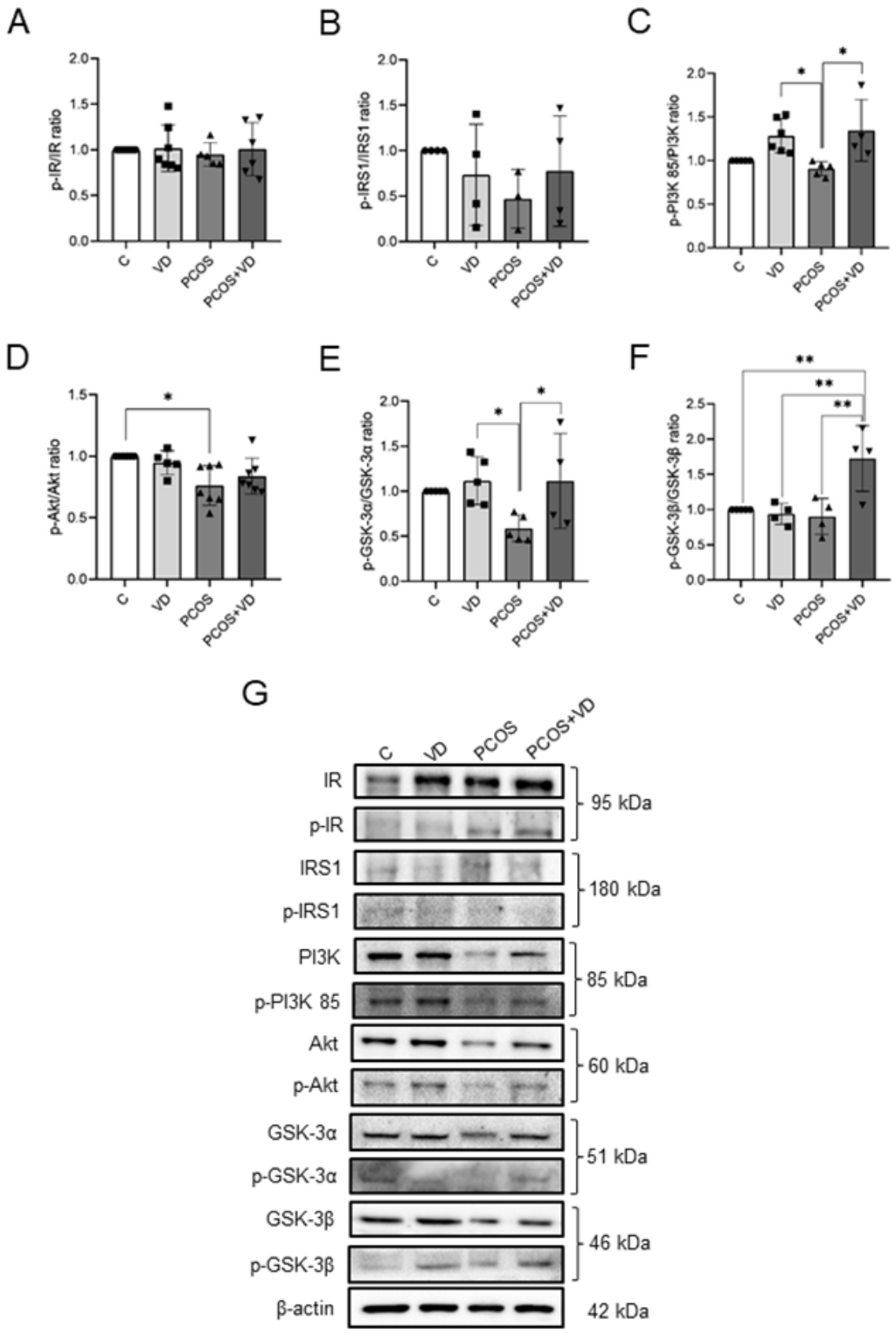

Figure 4. Western blot analysis of the phosphorylation of proteins involved in the intracellular signaling pathway activated by insulin in the uteri of rats from control (C), vitamin D_3-treated (VD), polycystic ovary syndrome-induced (PCOS) and PCOS-induced with vitamin D_3 supplementation (PCOS+VD) groups (n=8/group). Representative Western blots are shown (G). The relative protein abundance of total and phosphorylated forms was measured by densitometry and expressed as the ratio relative to β-actin. Each value represents the mean ± SD (standard deviation). Statistical analysis was carried out using one-way ANOVA followed by Tukey's test ($P<0.05$). IR, insulin receptor; p-IR, phospho-IR; IRS1, insulin receptor substrate 1; p-IRS1, phospho-IRS1; PI3K 85, phosphoinositide 3-kinase 85; p-PI3K, phospho-PI3K; Akt, protein kinase B, p-Akt, phospho-Akt; GSK-3α, glycogen synthase kinase-3α; p-GSK-3α, phospho-GSK-3α; GSK-3β, glycogen synthase kinase-3β; p-GSK-3β, phospho-GSK-3β

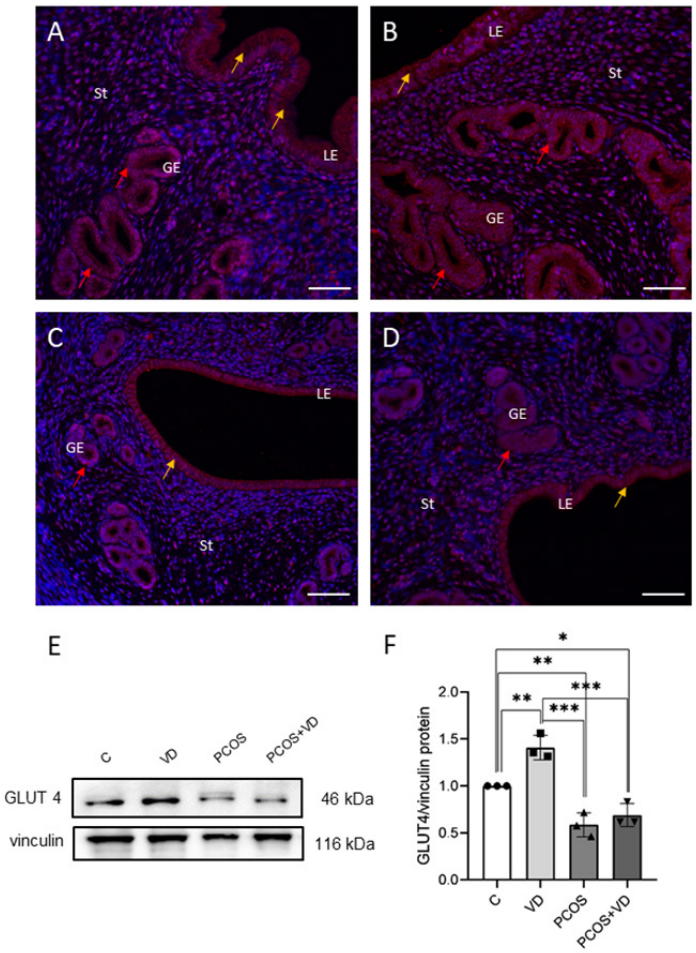

Figure 5. Immunofluorescent localization of Glut 4 in the uteri of rats from control (A), vitamin D_3-treated (B), polycystic ovary syndrome-induced (C) and PCOS-induced with vitamin D_3 supplementation (D) groups (n=8/group). Positive (red) reaction within luminal epithelium is marked by yellow arrows, and in the glandular epithelium by red arrows. DAPI staining (blue) is in the nucleus only. Negative control (D inset). GE, glandular epithelium; LE, luminal epithelium; St, stroma. Scale bar = 50 µm. Representative blots of Glut4 protein abundance (E) and its relative abundance measured by densitometry and expressed as the ratio relative to vinculin. Each value represents the mean ± SD (standard deviation). Statistical analysis was carried out using one-way ANOVA followed by Tukey's test ($P<0.05$)

In the C group, IR spectra indicate secretion of GAGs/PGs/GPs (1220 and 1238 cm^{-1}) and polysaccharides (1083 and 1060 cm^{-1}) within the uterine glands. In the VD group, there was a significant lowering of the 1238 and 1083 cm^{-1} signals, suggesting that some groups of sugar-amino acid conjugations were not synthesized along with polysaccharides containing the phosphate groups (Figure 1 C). In the PCOS group, region 1 showed the presence of a very specific collagen IR signature instead of GAGs/PGs/GPs, *i.e.*, bands at 1282, 1232, 1205 cm^{-1}. We also observed dysregulation of polysaccharides production since both bands in region 2 were shifted compared with the C group and exhibited similar intensity. The two spectral features implicated the synthesis of new sugars, mainly polysaccharides. In the PCOS+VD group, we found two different spectral profiles (PCOS+VD1 and PCOS+VD2; Figure 1 C). In the first group, glands still showed the presence of collagens, but GAGs/PGs/GPs were also produced again as a shoulder at 1238 cm^{-1}, while region 2 resembled the profile of the C and VD groups. Collagens disappeared completely in the PCOS+VD2 group and GAGs/PGs/GPs were secreted as in the C group (Figure 1 C). The additional difference between PCOS+VD1 and 2 was a significant decrease in the 1083 cm^{-1} band of polysaccharides.

Effect of VD on the insulin signaling pathway

Western blot analysis was performed to determine changes in the phosphorylation of proteins involved in the intracellular signaling pathway activated by insulin (Figure 4). There were no significant differences in the phosphorylation level of IR (Figure 4 A and G) and its substrate IRS1 (Figure 4 B and G). However, we noted markedly decreased phosphorylation of PI3K 85 kinase in the PCOS group in comparison to the VD and PCOS+VD groups (Figure 4 C and G; $P<0.05$). In the PCOS group, we also found the diminished level of Akt kinase phosphorylation when compared to the C group (Figure 4 D and G; $P<0.05$). Further analysis of GSK-3 (subunits α and β), which is a critical downstream target

of the insulin-stimulated PI3K/Akt signaling pathway, showed an increase in the phosphorylation of GSK-3α (Figure 4 E and G; P<0.05) and GSK-3β (Figure 4 F and G; P<0.01) in the PCOS+VD group when compared to the PCOS-induced group. In addition, the GSK-3α phosphorylation level was higher in the VD group than in the PCOS group (Figure 4 E and G; P<0.05), while GSK-3β phosphorylation was decreased in the C and VD groups in comparison with the PCOS-induced animals (Figure 4 F and G; P<0.01).

Effect of VD on GLUT4 localization and protein abundance

In the next step, we analyzed the cellular distribution (Figure 5 A–D) and protein abundance (Figure 5 E and F) of GLUT4, which is involved in the insulin-induced transport of glucose into the cells. The positive immunofluorescent signal was found within LE and GE of all examined groups (Figure 5 A–D). In the C (Figure 5 A) and VD (Figure 5 B) groups, both types of epithelia showed intensive GLUT4 staining; in the LE, GLUT4 distribution was cytoplasmic, while in the GE it was membranous. In the PCOS (Figure 5 C) and PCOS+VD (Figure 5 D) groups, only cytoplasmic GLUT4 immunoreaction was observed in both LE and GE, which was distinctly weaker within glands.

The abundance of GLUT 4 protein was significantly decreased in the PCOS and PCOS+VD groups in comparison with the C (P<0.01 and P<0.05, respectively) and VD (P<0.001) groups. Furthermore, VD increased (P<0.01) GLUT4 protein abundance when compared with the C group (Figure 5 E and F).

Discussion

In the present study, a letrozole-induced PCOS model with additional VD supplementation was used to investigate whether VD could be a promising tool in PCOS treatment by influencing uterine histoarchitecture, the biochemical composition of glandular fluid, and the insulin signal transduction pathway. As we showed in previous research on the same experimental model, successful PCOS induction was confirmed by rat acyclicity, high serum testosterone level and cysts in the ovaries (Pich et al., 2023).

In the current study, uterine size was significantly smaller and the thicknesses of the endometrium, myometrium, LE and GE were reduced following PCOS induction. In agreement, Haslan et al. (2021) demonstrated similar histomorphometric changes in letrozole-treated rats. However, other studies that utilized dehydroepiandrosterone (DHEA) for PCOS induction showed increased uterine weight and greater morphological parameters (Kuyucu et al., 2018; Bracho et al., 2019). Knowing that the uterus is a hormone-dependent tissue and that estrogens are mainly responsible for its growth and development (Weihua et al., 2002), the above discrepancies could be due to the hormonal imbalance present in different PCOS models. In DHEA-treated rats, the level of estradiol was higher (Kuyucu et al., 2018) or unchanged (Bracho et al., 2019) in comparison with control animals, whereas letrozole led to its decrease by aromatase inhibition (Li et al., 2017; Haslan et al., 2021; Pich et al., 2023). Regarding the effect of VD on uterine histoarchitecture in PCOS, we did not observe significantly ameliorating effects on the evaluated parameters. Noticeably, the endometrium thickness in the PCOS+VD group showed a tendency to be greater than in PCOS rats, and was similar to that from the VD group. As shown in infertile PCOS women, VD can restore endometrial thickness through induction of cell proliferation (Asadi et al., 2014). In the study by Kuyucu et al. (2018), VD improved some PCOS-caused endometrial changes, namely endometrium and stroma thickness, but not epithelium height that is partially consistent with the current findings. Thus, the beneficial effect of VD supplementation on endometrial parameters in PCOS seems to be plausible. However, the dose of VD and time of exposure could be limiting factors.

Uterine gland secretions play an important role in fertility and pregnancy success by influencing uterine receptivity and conceptus survival and growth (Kelleher et al., 2019). Their molecular profile varies with hormonal changes in different physiological/pathological states and may be used as a marker of uterine conditions (de Oliveira et al., 2015; Kelleher et al., 2019). Therefore, we have examined for the first time the biochemical composition of uterine secretions, showing pronounced changes in carbohydrate profiles during PCOS. In the C and VD groups, secretions in the lumen of glands and on the LE surface stained positively for acidic polysaccharides. Detailed FTIR analysis confirmed the presence of GAGs, PGs and GPs, which are important extracellular matrix molecules involved in cell proliferation, migration, adhesion and differentiation (de Oliveira et al., 2015), within the uterine glands of those animals. In both letrozole-treated groups, uterine gland secretions were stained for acidic and neutral polysaccharides, while no positive staining was found in the LE, probably due to the limited amount of secreted fluid. Based on FTIR spectra, the PCOS group displayed collagen-specific bands, altered position of bands attributed to GAGs, PGs and GPs, as well as shifted bands assigned to polysaccharides. That suggests the synthesis of new carbohydrates and explains the additional presence of PAS positive neutral polysaccharides in comparison to the C group. Since Kawakami et al. (2000) reported greater GAGs concentration in the ampulla and isthmus fluids, and in the lumen of uterine horns in bitches during the estrus phase than in the anestrus phase, a stimulating effect of estradiol on GAG level is proposed. Similarly, a study quantifying sulfated GAGs in the endometrium of PCOS women demonstrated a higher level of heparan sulfate related to persistent exposure to estradiol and endometrium hyperplasia (Giordano et al., 2015). This mechanism could explain the reduced

intensity of a spectral band assigned to GAGs in PCOS rats, displaying acyclicity and decreased estradiol levels (Pich et al., 2023). Considering the impact of VD on sugar composition in uterine gland secretions, two trends of response were observed in the PCOS+VD group. The first was represented by FTIR spectra similar to those in the C group, while the second was characterized by resynthesis of GAGs, PGs and GPs next to the presence of collagens. These results clearly indicate the beneficial role of VD in restoring the proper carbohydrate composition in uterine gland secretions, which is crucial for the maintenance of uterus functions in PCOS rats.

Clinical trials (He et al., 2015) and research on PCOS animal model (Grzesiak et al., 2021) revealed that besides hormonal and metabolic disturbances, VD deficiency is often related to PCOS. In accordance with this, diminished plasma 25OHD level occurred in the PCOS rats and VD supplementation withdrew this effect. Furthermore, we confirmed the development of hyperinsulinemia and insulin resistance, marked by increased insulin level and HOMA-IR after PCOS induction. Taken together, the combination of VD deficiency and insulin resistance in PCOS patients, as well as direct regulation of insulin synthesis by VD (Maestro et al., 2003), these results suggest that VD therapy may be useful in the reduction of insulin resistance in PCOS. In the PCOS+VD group, VD significantly decreased HOMA-IR, thereby improving insulin sensitivity. Similar effect occurred in an estradiol valerate-treated rat PCOS model (Behmanesh et al., 2019), in a letrozole-induced mouse PCOS model (Skarra et al., 2017) and in PCOS women (Gupta et al., 2017; Dastorani et al., 2018; Miao et al., 2020). Wehr et al. (2011) demonstrated ameliorated glucose metabolism in PCOS patients following VD administration, which is in agreement with our study showing diminished glucose levels in the PCOS+VD group. Furthermore, decreased glucose concentrations and increased HOMA-β in the VD group provide evidence for a direct action of VD on pancreatic β cells. To sum up, our experimental model confirms the ability of VD supplementation to overcome metabolic disturbances in PCOS, such as peripheral insulin resistance.

Recent studies showed a negative effect of hyperinsulinemia on endometrial functions in PCOS women (Zhao et al., 2023). In the uterus of letrozole-induced PCOS rats, differentially expressed miRNA were predicted to target genes associated with insulin secretion and intracellular signaling pathways, such as AMPK, PI3K/Akt and Ras (Li et al., 2017). In addition, pronounced changes in uterine morphology, especially within GE, were observed in rats with experimentally induced insulin resistance due to suppression of the PI3K/Akt and MAPK/ERK signaling pathways (Zhang et al., 2016). Therefore, the dysregulation of intracellular insulin signal transduction could be a possible mechanism of uterine histomorphometric changes in PCOS. Considering the positive effect of VD supplementation on peripheral insulin resistance in PCOS rats, the question arises of whether the insulin signaling pathway in the uterus is also influenced by VD treatment. In the PCOS group, insulin-mediated phosphorylation of IR and its substrate IRS1 were unaltered. The endometrium of PCOS women with hyperinsulinemia, had unchanged expression of IR, but decreased level of IRS1 (Fornes et al., 2010). However, that research was performed on the endometrium, whereas our study utilized the entire rat uterus. Furthermore, downstream activation of PI3K/Akt was inhibited here, in agreement with previous research by Li et al. (2017), indicating the development of local uterine insulin resistance in PCOS rats. The study on rat granulosa cells showed a positive effect of $1,25(OH)_2D_3$ on PI3K/Akt pathway activation *in vitro* (Lee et al., 2019). Accordingly, we have shown for the first time that VD supplementation increased PI3K phosphorylation and thereby might improve insulin resistance in the PCOS uterus.

Among various Akt target proteins are those involved in the metabolic cascade of the insulin signaling pathway, such as GSK-3, which is a key enzyme in the final step of glycogen synthesis and glucose metabolism. Akt phosphorylates GSK-3α on Ser21 and GSK-3β on Ser9 to render them inactive (Rahman et al., 2021). Upon VD treatment, the phosphorylation of both GSK-3α and GSK-3β isoforms was elevated in the PCOS uterus, which could further lead to GSK-3 inactivation and subsequent glucose deposition as glycogen, crucial for endometrial function and development (Oróstica et al., 2016). Interestingly, in the PCOS+VD group we did not observe changes in the protein abundance or cellular localization of GLUT4 responsible for glucose uptake. Diminished GLUT4 transcript and protein expression was found in the endometrium of PCOS women with hyperinsulinemia (Mioni et al., 2004; Mozzanega et al., 2004) in agreement with our findings from the PCOS group. Although GLUT4 is a major endometrial insulin-responsive glucose transporter, the expression of many different GLUT isoforms was confirmed in the rat uterus (Zhang et al., 2016). Thus, we cannot exclude the impact of VD on their expression to facilitate glucose uptake despite unaltered GLUT4 localization and abundance in the PCOS+VD. However this possibility requires further investigation.

In conclusion, our study demonstrates a role for VD in maintaining the proper sugar composition in uterine gland secretions without a pronounced effect on histomorphometric parameters in the uterus of PCOS rat model. Furthermore, VD supplementation may counteract local uterine insulin resistance through activation of the PI3K/Akt pathway and subsequent glucose metabolism, thereby improving uterine function in PCOS.

Conflict of interest

None of the authors has any conflict of interest to declare.

Acknowledgements

The authors would like to thank the Department of Comparative Anatomy, Institute of Zoology and Bio-

medical Research, Jagiellonian University for the opportunity to perform histological staining. The Authors are very grateful to Prof. Martin R. Luck (University of Nottingham) for English language correction.

The open-access publication of this article was funded by the programme "Excellence Initiative – Research University" at the Faculty of Biology of the Jagiellonian University in Kraków, Poland.

References

Asadi M., Matin N., Frootan M., Mohamadpour J., Qorbani M., Tanha F.D. (2014). Vitamin D improves endometrial thickness in PCOS women who need intrauterine insemination: a randomized double-blind placebo-controlled trial. Arch. Gynecol. Obstet., 289: 865–870.

Azziz R., Carmina E., Chen Z., Dunaif A., Laven J.S., Legro R.S., Lizneva D., Natterson-Horowtiz B., Teede H.J., Yildiz B.O. (2016). Polycystic ovary syndrome. Nat. Rev. Dis. Primers, 2: 16057.

Bavington C.D., Lever R., Mulloy B., Grundy M.M., Page C.P., Richardson N.V. McKenzie J.D. (2004). Anti-adhesive glycoproteins in echinoderm mucus secretions. Comp. Biochem. Physiol. B Biochem. Mol. Biol., 139: 607–617.

Behmanesh N., Abedelahi A., Charoudeh H.N., Alihemmati A. (2019). Effects of vitamin D supplementation on follicular development, gonadotropins and sex hormone concentrations, and insulin resistance in induced polycystic ovary syndrome. Turk. J. Obstet. Gynecol., 16: 143–150.

Bracho G.S., Altamirano G.A., Kass L., Luque E.H., Bosquiazzo V.L. (2019). Hyperandrogenism induces histoarchitectural changes in the rat uterus. Reprod. Sci., 26: 657–668.

Dastorani M., Aghadavod E., Mirhosseini N., Foroozanfard F., Zadeh Modarres S., Amiri Siavashani M., Asemi Z. (2018). The effects of vitamin D supplementation on metabolic profiles and gene expression of insulin and lipid metabolism in infertile polycystic ovary syndrome candidates for in vitro fertilization. Reprod. Biol. Endocrinol., 16: 94.

de Oliveira G.B., do Vale A.M., dos Santos A.C., de Moura C.E.B., de Oliveira Rocha H.A., de Oliveira M.F. (2015). Composition and significance of glycosaminoglycans in the uterus and placenta of mammals. Braz. Arch. Biol. Technol., 58: 512–520.

Fornes R., Ormazabal P., Rosas C., Gabler F., Vantman D., Romero C., Vega M. (2010). Changes in the expression of insulin signaling pathway molecules in endometria from polycystic ovary syndrome women with or without hyperinsulinemia. Mol. Med., 16: 129–136.

Giordano M.V., Giordano L.A., Gomes R.C., Simões R.S., Nader H.B., Giordano M.G., Baracat E.C., Soares Júnior J.M. (2015). The evaluation of endometrial sulfate glycosaminoglycans in women with polycystic ovary syndrome. Gynecol. Endocrinol., 31: 278–281.

Grzesiak M., Burzawa G., Kurowska P., Blaszczyk K., Szlaga A., Blasiak A., Sechman A., Rak A. (2021). Altered vitamin D_3 metabolism in the ovary and periovarian adipose tissue of rats with letrozole-induced PCOS. Histochem. Cell Biol., 155: 101–116.

Grzesiak M., Kaminska K., Bodzioch A., Drzewiecka E.M., Franczak A., Knapczyk-Stwora K. (2022). Vitamin D_3 metabolic enzymes in the porcine uterus: expression, localization and autoregulation by $1,25(OH)_2D_3$ *in vitro*. Int. J. Mol. Sci., 23: 3972.

Gupta T., Rawat M., Gupta N., Arora S. (2017). Study of effect of vitamin D supplementation on the clinical, hormonal and metabolic profile of the PCOS women. J. Obstet. Gynaecol. India, 67: 349–355.

Haslan M.A., Samsulrizal N., Hashim N., Zin N.S.N.M., Shirazi F.H., Goh Y.M. (2021). *Ficus deltoidea* ameliorates biochemical, hormonal, and histomorphometric changes in letrozole-induced polycystic ovarian syndrome rats. BMC Complement. Med. Ther., 21: 291.

He C., Lin Z., Robb S.W., Ezeamama A.E. (2015). Serum vitamin D levels and polycystic ovary syndrome: a systematic review and meta-analysis. Nutrients, 7: 4555–4577.

Hosseinzadeh P., Barsky M., Gibbons W.E., Blesson C.S. (2021). Polycystic ovary syndrome and the forgotten uterus. F. S. Rev., 2: 11–20.

Jiang N.X., Li X.L. (2022). The disorders of endometrial receptivity in PCOS and its mechanisms. Reprod. Sci., 29: 2465–2476.

Kafali H., Iriadam M., Ozardali I., Demir N. (2004). Letrozole-induced polycystic ovaries in the rat: a new model for cystic ovarian disease. Arch. Med. Res., 35: 103–108.

Kalamon N., Błaszczyk K., Szlaga A., Billert M., Skrzypski M., Pawlicki P., Górowska-Wójtowicz E., Kotula-Balak M., Błasiak A., Rak A. (2020). Levels of the neuropeptide phoenixin-14 and its receptor GRP173 in the hypothalamus, ovary and periovarian adipose tissue in rat model of polycystic ovary syndrome. Biochem. Biophys. Res. Commun., 528: 628–635.

Kaminska K., Grzesiak M. (2021) The relationship between vitamin D_3 and insulin in polycystic ovary syndrome – a critical review. J. Physiol. Pharmacol., 72: 13–22.

Kawakami E., Arai T., Oishi I., Hori T., Tsutsui T. (2000). Induction of dog sperm capacitation by glycosaminoglycans and glycosaminoglycan amounts of oviductal and uterine fluids in bitches. J. Vet. Med. Sci., 62: 65–68.

Kelleher A.M., DeMayo F.J., Spencer T.E. (2019). Uterine glands: developmental biology and functional roles in pregnancy. Endocr. Rev., 40: 1424–1445.

Kuyucu Y., Çelik L.S., Kendirlinan Ö., Tap Ö., Mete U.Ö. (2018). Investigation of the uterine structural changes in the experimental model with polycystic ovary syndrome and effects of vitamin D treatment: An ultrastructural and immunohistochemical study. Reprod. Biol., 18: 53–59.

Lajtai K., Nagy C.T., Tarszabó R., Benkő R., Hadjadj L., Sziva R.E., Gerszi D., Bányai B., Ferdinandy P., Nádasy G.L., Giricz Z., Horváth E.M., Várbíró S. (2019). Effects of vitamin D deficiency on proliferation and autophagy of ovarian and liver tissues in a rat model of polycystic ovary syndrome. Biomolecules, 9: 471.

Lee C.T., Wang J.Y., Chou K.Y., Hsu M.I. (2019). 1,25-dihydroxyvitamin D_3 modulates the effects of sublethal BPA on mitochondrial function via activating PI3K-Akt pathway and 17β-estradiol secretion in rat granulosa cells. J. Steroid. Biochem. Mol. Biol., 185: 200–211.

Lewis A.T., Jones K., Lewis K.E., Jones S., Lewis P.D. (2013). Detection of Lewis antigen structural change by FTIR spectroscopy. Carbohydr. Polym., 92: 1294–1301.

Li C., Chen L., Zhao Y., Chen S., Fu L., Jiang Y., Gao S., Liu Z., Wang F., Zhu X., Rao J., Zhang J., Zhou X. (2017). Altered expression of miRNAs in the uterus from a letrozole-induced rat PCOS model. Gene, 598: 20–26.

Li Y., Chen C., Ma Y., Xiao J., Luo G., Li Y., Wu D. (2019). Multi-system reproductive metabolic disorder: significance for the pathogenesis and therapy of polycystic ovary syndrome (PCOS). Life Sci., 228: 167–175.

Maestro B., Dávila N., Carranza M.C., Calle C. (2003). Identification of a vitamin D response element in the human insulin receptor gene promoter. J. Steroid. Biochem. Mol. Biol., 84: 223–230.

Miao C.Y., Fang X.J., Chen Y., Zhang Q. (2020). Effect of vitamin D supplementation on polycystic ovary syndrome: A meta-analysis. Exp. Ther. Med., 19: 2641–2649.

Mioni R., Chiarelli S., Xamin N., Zuliani L., Granzotto M., Mozzanega B., Maffei P., Martini C., Blandamura S., Sicolo N., Vettor R. (2004). Evidence for the presence of glucose transporter 4 in the endometrium and its regulation in polycystic ovary syndrome patients. J. Clin. Endocrinol. Metab., 89: 4089–4096.

Mohamed H.T., Untereiner V., Cinque G., Ibrahim S.A., Götte M., Nguyen N.Q., Rivet R., Sockalingum G.D., Brézillon S. (2020). Infrared microspectroscopy and imaging analysis of inflammatory and non-inflammatory breast cancer cells and their GAG secretome. Molecules**,** 25: 4300.

Moustafa S.R., Jebur I.M., Hasan M.A., Al-Nimer M.S. (2021). Serum magnesium and visfatin levels in newly diagnosed non-obese type

2 diabetes without insulin resistance: a cross-sectional study. Clin. Diab., 10: 123–128.

Mozzanega B., Mioni R., Granzotto M., Chiarelli S., Xamin N., Zuliani L., Sicolo N., Marchesoni D., Vettor R. (2004). Obesity reduces the expression of GLUT4 in the endometrium of normoinsulinemic women affected by the polycystic ovary syndrome. Ann. N. Y. Acad. Sci., 1034: 364–374.

Oróstica L., Rosas C., Plaza-Parrochia F., Astorga I., Gabler F., García V., Romero C., Vega M. (2016). Altered steroid metabolism and insulin signaling in PCOS endometria: impact in tissue function. Curr. Pharm. Des., 22: 5614–5624.

Pich K., Rajewska J., Kamińska K., Tchurzyk M., Szlaga A., Sambak P., Błasiak A., Grzesiak M., Rak A. (2023). Effect of vitamin D_3 on chemerin and adiponectin levels in uterus of polycystic ovary syndrome rats. Cells, 12: 2026.

Piltonen T.T. (2016). Polycystic ovary syndrome: Endometrial markers. Best. Pract. Res. Clin. Obstet. Gynaecol., 37: 66–79.

Rahman M.S., Hossain K.S., Das S., Kundu S., Adegoke E.O., Rahman M.A., Hannan M.A., Uddin M.J., Pang M.G. (2021). Role of insulin in health and disease: An update. Int. Mol. J. Sci., 22: 6403.

Sajadi M., Noroozzadeh M., Bagheripour F., Ramezani Tehrani F. (2018). Contractions in the isolated uterus of a rat model of polycystic ovary syndrome compared to controls in adulthood. Int. J. Endocrinol. Metab., 16: e63135.

Servaty R., Schiller J., Binder H., Arnold K. (2001). Hydration of polymeric components of cartilage – an infrared spectroscopic study on hyaluronic acid and chondroitin sulfate. Int. J. Biol. Macromol., 28: 121–127.

Skarra D.V., Hernández-Carretero A., Rivera A.J., Anvar A.R., Thackray V.G. (2017). Hyperandrogenemia induced by letrozole treatment of pubertal female mice results in hyperinsulinemia prior to weight gain and insulin resistance. Endocrinology, 158: 2988–3003.

Spremović Rađenović S., Pupovac M., Andjić M., Bila J., Srećković S., Gudović A., Dragaš B., Radunović N. (2022). Prevalence, risk factors, and pathophysiology of nonalcoholic fatty liver disease (NAFLD) in women with polycystic ovary syndrome (PCOS). Biomedicines, 10: 131.

Staniszewska E., Malek K., Baranska M. (2014). Rapid approach to analyze biochemical variation in rat organs by ATR FTIR spectroscopy. Spectrochim. Acta A Mol. Biomol. Spectrosc., 118: 981–986.

Wehr E., Pieber T.R., Obermayer-Pietsch B. (2011). Effect of vitamin D_3 treatment on glucose metabolism and menstrual frequency in polycystic ovary syndrome women: a pilot study. J. Endocrinol. Invest., 34: 757–763.

Weihua Z., Ekman J., Almkvist A., Saji S., Wang L., Warner M., Gustafsson J.A. (2002). Involvement of androgen receptor in 17beta-estradiol-induced cell proliferation in rat uterus. Biol. Reprod., 67: 616–623.

Wiercigroch E., Szafraniec E., Czamara K., Pacia M.Z., Majzner K., Kochan K., Kaczor A., Baranska M., Malek K. (2017). Raman and infrared spectroscopy of carbohydrates: A review. Spectrochim. Acta A Mol. Biomol. Spectrosci., 185: 317–335.

Zhang Y., Sun X., Sun X., Meng F., Hu M., Li X., Li W., Wu X.K., Brännström M., Shao R., Billig H. (2016). Molecular characterization of insulin resistance and glycolytic metabolism in the rat uterus. Sci. Rep., 6: 30679.

Zhao H., Zhang J., Cheng X., Nie X., He B. (2023). Insulin resistance in polycystic ovary syndrome across various tissues: an updated review of pathogenesis, evaluation, and treatment. J. Ovarian Res., 16: 9.

Received: 19 IX 2023
Accepted: 21 II 2024